Discrete vortex method for a detached flow on a two-airfoil configuration at high angle of attack

Thierry M. Faure, Vincent Drouet, Olivier Montagnier

52nd 3AF International Conference on Applied Aerodynamics
27 – 29 March 2017, Lyon - France

FP07-AERO2017-faure

DISCRETE VORTEX METHOD FOR A DETACHED FLOW ON A TWO-AIRFOIL CONFIGURATION AT HIGH ANGLE OF ATTACK

Thierry M. Faure (1), Vincent Drouet (1), Olivier Montagnier (1,2)
(1) Centre de Recherche de l'Armée de l'air, École de l'Air, B.A. 701, 13661 Salon-de-Provence, France, Email: thierry.faure@defense.gouv.fr
(2) Laboratoire de Mécanique et d'Acoustique, Aix-Marseille Université, Centre National de la Recherche Scientifique, Unité Propre de Recherche 7051, Centrale Marseille, 4 impasse Nicola Tesla, 13453 Marseille Cedex 13, France

ABSTRACT

Airfoils with high values of the angle of attack present detached flows, characterized by leading edge and trailing edge vortex shedding. Experiments and high-order computations contribute to the understanding of these flows, but fast low-order methods are needed for engineering tasks. In the present work, we implement a discrete-time vortex method, using a leading edge shedding criterion. For a given airfoil and Reynolds number, there is a critical value of that parameter. If the instantaneous value exceeds the critical value, vortex shedding occurs at the leading edge. In addition, the Kelvin theorem imposes for each time step, that the total circulation equals zero. That type of method, initially developed for flows around unsteady airfoils, is used to compute the unsteady flow resulting from detached airfoils at constant angle of attack. The airfoil configuration consists in two SD7003 airfoils of equal chord, placed at different stagger and gap. The study focuses on lift change produced varying the stagger between the airfoils.

1. INTRODUCTION

Unsteady aerodynamics of airfoils in incompressible flow, operated on moderate Reynolds numbers in the range 10^4 to 10^5, has gained in importance, for unmanned air vehicles (UAV) and micro air vehicles (MAV) applications [1]. Fixed-wing MAV need to fly at conditions close to the stall point, and post-stall flight would occur during maneuvers. Hence, delaying stall and improving performance for large values of the angle of attack is necessary. To do so, two-wing configurations are proposed as a means of generating large enough lift coefficient and delaying stall by controlling the flow. The present investigation focuses on the understanding of two-dimensional effects. The interaction between two airfoils is a key mechanism of flow control, with wakes and vortex shedding effects. Computational fluid dynamics is a classical way to address that issue, but low-order unsteady methods are useful and reliable options for engineering purpose. These methods have been developed some forty years ago, with limited application because of the small computer performance at that time [2]. However, with the advance of computing power, low-order numerical methods are a good balance between fidelity and cost. The present method is an unsteady airfoil theory based on potential flows, initially developed for flapping airfoil motion but applied hereafter to predict the unsteady detached flow on a static airfoil. After validating the algorithm on a single airfoil from low to high values of the angle of attack, the periodic characteristic of the vortex shedding are compared with experimental results. The method is then adapted to the case of two airfoils in interaction. The lift efficiency ratios are compared for different stagger and gap between the airfoils.

2. LEADING EDGE SUCTION PARAMETER DISCRETE VORTEX METHOD

The Leading edge suction parameter Discrete Vortex Method (LDVM) is based on the potential thin airfoil theory in unsteady flows, applicable for large values of the angle of attack [3]. It is built on the time-stepping approach of [4] with the addition of a criterion for the leading edge detachment. In figure 1, the aerodynamic frame (X,Z) is fixed and the airfoil frame (x,z) moves with a velocity U_∞ opposite to the X axis with a time-dependant angle of attack $\alpha(t)$. No motion along the Z axis is considered hereafter. The fluid velocity components are respectively U and W in the

aerodynamic frame and w is the velocity along z in the airfoil frame. The local circulation distribution over the airfoil is obtained from a Fourier series:

$$\gamma(\theta,t)=2U_\infty\left[A_0(t)\frac{1+\cos\theta}{\sin\theta}+\sum_{n=1}^{\infty}A_n(t)\sin n\theta\right] \quad (1)$$

with $A_0(t)$, … , $A_n(t)$ the time-dependant Fourier coefficients, c the airfoil chord and where:

$$x=\frac{c}{2}(1-\cos\theta) \quad (2)$$

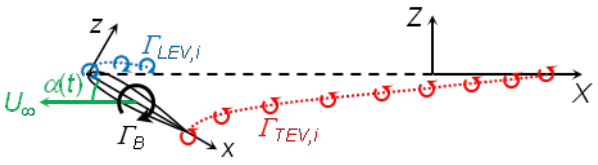

Figure 1. Airfoil motion and frames of reference.

The Kutta condition is enforced through the form of the Fourier series. The Fourier coefficients are determined from the instantaneous local downwash $w(\theta,t)$ by enforcing the potential flow boundary condition that the velocity is tangential to the airfoil surface:

$$A_0(t)=-\frac{1}{\pi}\int_0^\pi\frac{w(\theta,t)}{U_\infty}d\theta \quad (3)$$

$$A_n(t)=\frac{2}{\pi}\int_0^\pi\frac{w(\theta,t)}{U_\infty}\cos n\theta\, d\theta \quad (4)$$

where $w(\theta,t)$ is the velocity normal to the airfoil calculated from the motion kinematics:

$$w(\theta,t)=\frac{\partial\eta}{\partial x}\left(U_\infty\cos\alpha+\frac{\partial\Phi_B}{\partial x}+\frac{\partial\Phi_{TEV}}{\partial x}+\frac{\partial\Phi_{LEV}}{\partial x}\right) \quad (5)$$
$$-U_\infty\sin\alpha-\dot{\alpha}x-\frac{\partial\Phi_{TEV}}{\partial x}-\frac{\partial\Phi_{LEV}}{\partial x}$$

with Φ_B, Φ_{TEV}, Φ_{LEV} the velocity potentials associated with the bound, leading edge and trailing edge circulations and η the airfoil mean camber line. At each time step, if the flow around the airfoil is attached, a trailing edge vortex (TEV) is released and advected by the flow at the following time step. However, a separation model is needed for large values of the angle of attack. The separation on the airfoil is obtained with an inviscid parameter developed by [3]. The Leading Edge Suction Parameter (LESP) is a non-dimensional measure of the suction at the leading edge, and equates the first Fourier coefficient:

$$\mathrm{LESP}(t)=A_0(t) \quad (6)$$

The critical value LESP_{crit} corresponds to the A_0 value associated with the angle of attack for which a peak of pressure coefficient is reached at the leading edge. It is a measure of the maximum suction that a given airfoil can bear before separation and is independent of the motion. Beyond that LESP_{crit} value, the airfoil suction side boundary layer separates from the leading edge, which corresponds to the release of a leading edge vortex (LEV). In that case, there is shedding of both a TEV and a LEV. This situation is illustrated in figure 1 for the iteration step i, which is the first one with the LESP exceeding its critical value, and with the release of two vortices. These ones, at every time step, must enforce Kelvin's circulation theorem:

$$\Gamma_B(t)+\sum_{k=1}^{i}\Gamma_{TEV,k}+\sum_{l=1}^{i}\Gamma_{LEV,l}=0 \quad (7)$$

With the airfoil bound circulation:

$$\Gamma_B(t)=\int_0^\pi\gamma(\theta,t)d\theta=U_\infty c\pi\left[A_0(t)+\frac{A_1(t)}{2}\right] \quad (8)$$

The previous variables are written in a non-dimensional form as:

$$w^*=\frac{w}{U_\infty}\quad U^*=\frac{w}{U_\infty}\quad W^*=\frac{W}{U_\infty}$$
$$X^*=\frac{X}{c}\quad Z^*=\frac{Z}{c}\quad \Gamma^*=\frac{\Gamma}{U_\infty c} \quad (9)$$

The velocity induced by a given vortex is described with the model of Vatistas which incorporates a finite core radius r_c [5]:

$$U_k^*=\frac{\Gamma_k^*}{2\pi}\frac{Z^*-Z_k^*}{\sqrt{\left[\left(X^*-X_k^*\right)^2+\left(Z^*-Z_k^*\right)^2\right]^2+r_c^{*4}}}$$
$$W_k^*=-\frac{\Gamma_k^*}{2\pi}\frac{X^*-X_k^*}{\sqrt{\left[\left(X^*-X_k^*\right)^2+\left(Z^*-Z_k^*\right)^2\right]^2+r_c^{*4}}} \quad (10)$$

The non-dimensional time step is:

$$\delta t^*=\frac{\delta t U_\infty}{c}=0.015 \quad (11)$$

The vortex core radius is taken to be 1.3 times the average spacing between the vortices [6]:

$$r_c^*=\frac{r_c}{c}=1.3\delta t^*=0.02 \quad (12)$$

The last shed vortex is placed at one-third of the distance from the shedding edge to the previously shed vortex [7]:

$$X_{TEV,k}^*=X_{TE}^*+\frac{1}{3}\left(X_{TEV,k-1}^*-X_{TE}^*\right)$$
$$Z_{TEV,k}^*=Z_{TE}^*+\frac{1}{3}\left(Z_{TEV,k-1}^*-Z_{TE}^*\right)$$
$$X_{LEV,l}^*=X_{LE}^*+\frac{1}{3}\left(X_{LEV,l-1}^*-X_{LE}^*\right) \quad (13)$$
$$Z_{LEV,l}^*=Z_{LE}^*+\frac{1}{3}\left(Z_{LEV,l-1}^*-Z_{LE}^*\right)$$

For each time-step, the unknown parameters are the circulations corresponding to the newly shed vortices, advected by the velocity field. Firstly, if there is only a TEV shed at the iteration i, equation (5) is reduced to:

$$w^*\left(\theta,t_i^*\right)=T_1+\Gamma_{TEV,i}^*T_2 \quad (14)$$

where T_1 and T_2 are terms depending on the angle of attack and the summation of the influence of the previously shed vortices. The only unknown parameter is the circulation of the TEV shed at iteration *i*. The airfoil bound circulation is obtained from (8) substituting the Fourier coefficients:

$$\begin{aligned}\Gamma_B^* &= \int_0^\pi T_1(\cos\theta - 1)d\theta + \Gamma_{TEV,i}^* \int_0^\pi T_2(\cos\theta - 1)d\theta \\ &= I_1 + I_2\Gamma_{TEV,i}^*\end{aligned} \tag{15}$$

Substituting (15) into Kelvin's theorem (7):

$$\Gamma_{TEV,i}^* = -\frac{I_1 + \sum_{k=1}^{i-1}\Gamma_{TEV,k}^* + \sum_{l=1}^{i-1}\Gamma_{TEV,l}^*}{1 + I_2} \tag{16}$$

Secondly, if both a TEV and LEV are shed at iteration *i*, then equation (5) is reduced to:

$$w^*(\theta, t_i^*) = T_1 + \Gamma_{TEV,i}^* T_2 + \Gamma_{LEV,i}^* T_3 \tag{17}$$

where T_1, T_2 and T_3 are terms depending on the angle of attack and the summation of the influence of the previously shed vortices. There is two unknown parameters which are the circulations of the TEV and LEV shed at iteration *i*, requiring two equations. The airfoil bound circulation is obtained from (8) substituting the Fourier coefficients:

$$\Gamma_B^* = J_1 + J_2\Gamma_{TEV,i}^* + J_3\Gamma_{LEV,i}^* \tag{18}$$

where J_1, J_2 and J_3 are terms resulting of the integrals of T_1, T_2 and T_3. Kelvin's theorem (7) and the criterion on the critical LESP provide:

$$\begin{aligned}&\Gamma_B^* + \Gamma_{TEV,i}^* + \Gamma_{LEV,i}^* + \sum_{k=1}^{i-1}\Gamma_{TEV,k}^* + \sum_{l=1}^{i-1}\Gamma_{LEV,l}^* = 0 \\ &A_0 - \mathrm{LESP}_{crit} = 0\end{aligned} \tag{19}$$

Substituting the bound circulation and the value of A_0, equation (19) is:

$$\begin{aligned}&J_1 + \Gamma_{TEV,i}^*(1 + J_2) + \Gamma_{LEV,i}^*(1 + J_3) + \sum_{k=1}^{i-1}\Gamma_{TEV,k}^* \\ &+ \sum_{l=1}^{i-1}\Gamma_{LEV,l}^* = 0 \\ &I_1 + I_2\Gamma_{TEV,i}^* + I_3\Gamma_{LEV,i}^* - \mathrm{LESP}_{crit} = 0\end{aligned} \tag{20}$$

Note that this is a linear system, and no iteration scheme is required as previously mentioned in [3] and [4]. Therefore, a significant gain in calculation time is expected. As only the shed LEV and TEV are computed with the method, it is worth noticing that the simulation time is increasing with the number of vortices. In order to reduce that number, the vortices located four chords downstream of the leading edge can be amalgamated into larger structures [2]. That clustering can be realized with a multidimensional binary search tree or k-d tree [8], for all the vortices downstream of four chord of the airfoil.

3. AERODYNAMIC COEFFICIENTS

The unsteady form of the Bernoulli theorem is used to calculate the pressure distribution along the airfoil:

$$p_{ps} - p_{ss} = \rho\left[\frac{1}{2}\left(V_{t,ss}^2 - V_{t,ps}^2\right) + \frac{\partial\Phi_{ss}}{\partial t} - \frac{\partial\Phi_{ps}}{\partial t}\right] \tag{21}$$

with the indices *ps* and *ss* respectively for the pressure side and suction side and V_t the tangential velocity. As the flow potential function is the sum of the potential functions of the bound circulation, TEV and LEV:

$$\Phi = \Phi_B + \Phi_{TEV} + \Phi_{LEV} \tag{22}$$

the tangential velocity is:

$$\begin{aligned}V_{t,ss} &= U_\infty\cos\alpha + \left(\frac{\partial\Phi_B}{\partial x}\right)_{ss} + \left(\frac{\partial\Phi_{TEV}}{\partial x}\right)_{ss} \\ &+ \left(\frac{\partial\Phi_{LEV}}{\partial x}\right)_{ss} \\ V_{t,ps} &= U_\infty\cos\alpha + \left(\frac{\partial\Phi_B}{\partial x}\right)_{ps} + \left(\frac{\partial\Phi_{TEV}}{\partial x}\right)_{ps} \\ &+ \left(\frac{\partial\Phi_{LEV}}{\partial x}\right)_{ps}\end{aligned} \tag{23}$$

From the thin airfoil theory:

$$\left(\frac{\partial\Phi_B}{\partial x}\right)_{ss} = \frac{\gamma(x,t)}{2} \qquad \left(\frac{\partial\Phi_B}{\partial x}\right)_{ps} = -\frac{\gamma(x,t)}{2} \tag{24}$$

Then:

$$\begin{aligned}&V_{t,ss}^2 - V_{t,ps}^2 = \\ &2\left[U_\infty\cos\alpha + \frac{\partial\Phi_{TEV}}{\partial x} + \frac{\partial\Phi_{LEV}}{\partial x}\right]\gamma(x,t)\end{aligned} \tag{25}$$

The potential functions time derivatives are:

$$\frac{\partial\Phi_{ss}}{\partial t} - \frac{\partial\Phi_{ps}}{\partial t} = \frac{\partial}{\partial t}\int_0^x\gamma(\xi,t)d\xi \tag{26}$$

Hence (21) becomes:

$$\begin{aligned}p_{ps} - p_{ss} = \rho\Bigg\{&\left[U_\infty\cos\alpha + \frac{\partial\Phi_{TEV}}{\partial x}\right. \\ &\left. + \frac{\partial\Phi_{LEV}}{\partial x}\right]\gamma(x) + \frac{\partial}{\partial t}\int_0^x\gamma(\xi,t)d\xi\Bigg\}\end{aligned} \tag{27}$$

The normal force on the airfoil is obtained:

$$\begin{aligned}F_N = \rho\Bigg[&\int_0^c\left(U_\infty\cos\alpha + \frac{\partial\Phi_{TEV}}{\partial x}\right. \\ &\left. + \frac{\partial\Phi_{LEV}}{\partial x}\right)\gamma(x,t)d\xi + \int_0^c\frac{\partial}{\partial t}\int_0^x\gamma(\xi,t)d\xi dx\Bigg]\end{aligned} \tag{28}$$

Using the Fourier coefficients, it is reduced to:

$$\begin{aligned}F_N = \rho U_\infty c\pi\Bigg[&U_\infty\cos\alpha\left(A_0 + \frac{A_1}{2}\right) + c\left(\frac{3\dot{A}_0}{4}\right. \\ &\left. + \frac{\dot{A}_1}{4} + \frac{\dot{A}_2}{8}\right) + \rho\int_0^c\left(\frac{\partial\Phi_{TEV}}{\partial x} + \frac{\partial\Phi_{LEV}}{\partial x}\right)\gamma(x,t)dx\Bigg]\end{aligned} \tag{29}$$

The axial force is given by the Blasius formula [4]:

$$F_A = \rho U_\infty^2 c \pi A_0^2 \tag{30}$$

Similarly, the moment about the position x_{ref} on the airfoil is:

$$M = x_{ref} F_N - \rho U_\infty c^2 \pi \left[U_\infty \cos\alpha \left(\frac{A_0}{4} + \frac{A_1}{4} - \frac{A_2}{8} \right) + c \left(\frac{7\dot{A}_0}{16} + \frac{3\dot{A}_1}{16} + \frac{\dot{A}_2}{16} - \frac{\dot{A}_3}{64} \right) - \rho \int_0^c \left(\frac{\partial \Phi_{TEV}}{\partial x} + \frac{\partial \Phi_{LEV}}{\partial x} \right) \gamma(x,t) x dx \right] \tag{31}$$

4. UNSTEADY MOTION

The present algorithm is tested for unsteady motions on the cases 1, 5A and 5B of [3]. They are respectively a pitch-hold-return motion of a SD7003 airfoil at a Reynolds number $Re = 30000$ (case 1) and pitch-up maneuvers of a flat plate at $Re = 1000$ (cases 5A and 5B). Figure 2 shows the results for case 1, where each LEV or TEV is represented by a color dot in blue (respectively red) for a clockwise (respectively counter-clockwise) circulation. The time development of the shedding vortices is exactly identical as in [3]. The aerodynamic coefficients are given in figure 3. The variation with time of the angle of attack is an increasing and decreasing ramp between 0° and 25° (figure 3-a). The lift, drag and moment about the quarter chord coefficients are compared with LDVM computations of [3], experiments and CFD (figure 3-b to d). An excellent agreement is observed between the two LDVM, and the deviation between the present computation and the experiment or CFD is not larger than what is found in [3]. The same comments are valid for cases 5A and 5B.

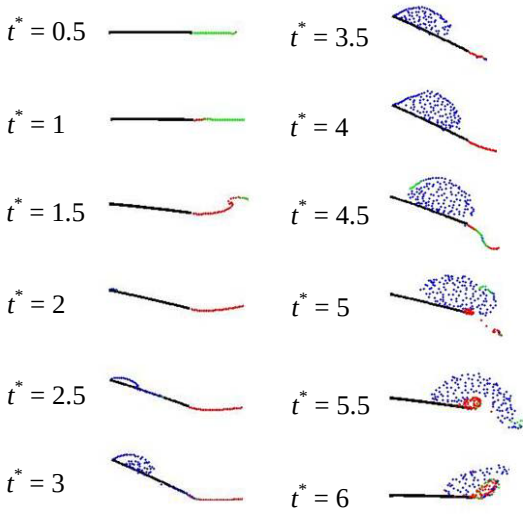

Figure 2. Flow features for case 1 (airfoil SD7003, $Re = 30000$, pitch-hold-return motion).

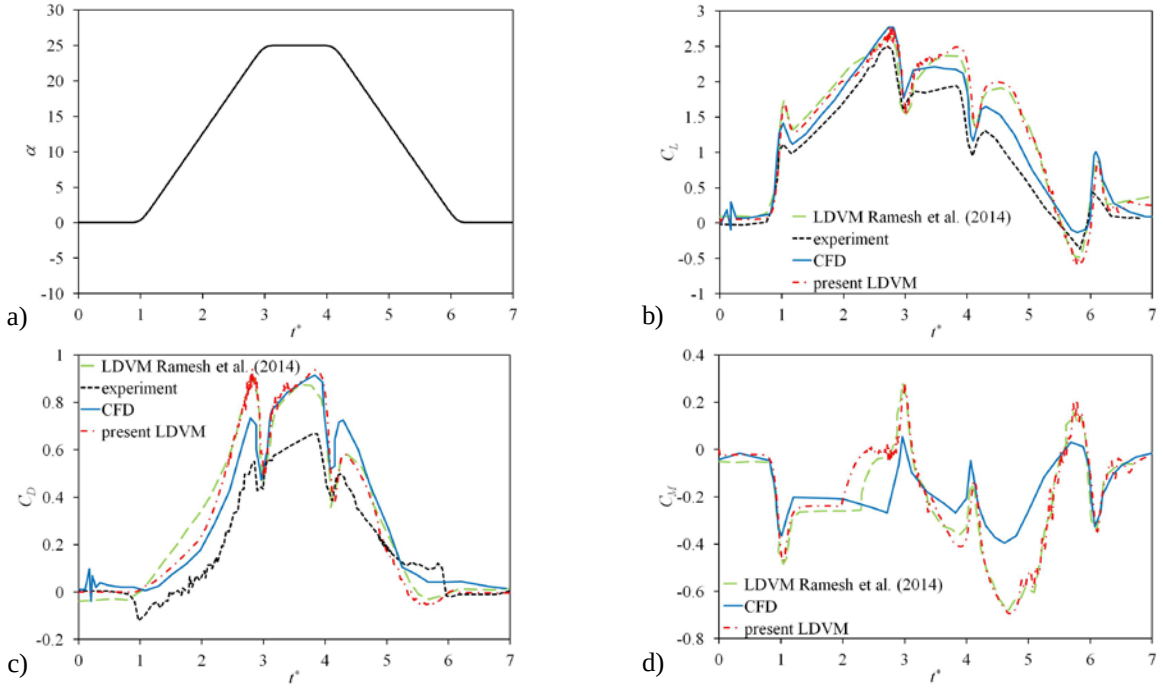

Figure 3. Case 1 of the unsteady motion [3], variation with t^* of : a) angle of attack, b) lift coefficient from LDVM, experiment and CFD, c) drag coefficient from LDVM, experiment and CFD, d) pitching-moment about the quarter chord from LDVM and CFD.

5. SINGLE AIRFOIL CONFIGURATION

The present study applies the LDVM to the unsteady flow developing around a steady airfoil. In order to get the critical value of the LESP, a SD7003 airfoil is chosen because the development of that parameter with Reynolds number is published in [9], and equals 0.149 for the selected value $Re = 10^5$. For each run, corresponding to a given value of the angle of attack, 15000 iterations are performed. Figure 4 shows the lift, drag and pitching moment about the quarter-chord coefficients versus angle of attack. The agreement of the lift coefficient obtained with the LDVM and the thin airfoil theory is excellent as long as the flow is attached between -10° and 10°. Experimental results at $Re = 10^5$ [10] and CFD performed at $Re = 6\times10^4$ [11] are also plotted in the figure. The agreement is good up to the stall angle, which is around 11°. Then, the plateau observed in the experiment and CFD is found, but with values greater by 30%. A good agreement is observed on the drag coefficient. Note that the LDVM is able to predict the aerodynamic coefficients far beyond the stall point, where available data are usually limited to.

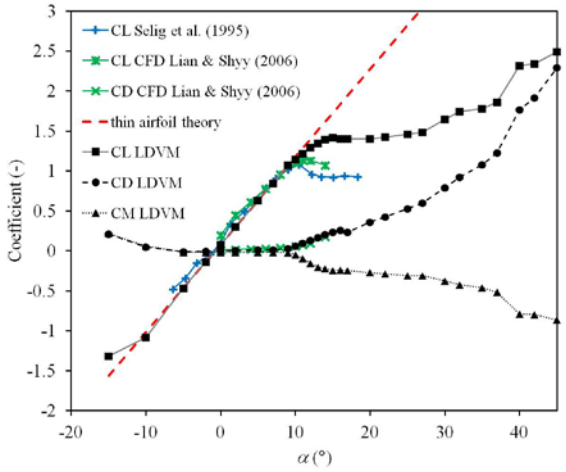

Figure 4. Lift, drag and moment about the quarter-chord coefficients for a SD7003 airfoil.

Figure 5 presents the flow development for an angle of attack of 35° at a simulation time $t^* = 220$, with no vortex clustering. Note that the airfoil suction side is completely detached, with a well-defined detachment line from the leading edge. Periodic shedding is observed downstream of the airfoil, each individual vortex core developing into larger structures. That vortex shedding is also inducing time modulation of the aerodynamic coefficients. Figure 6 is the time development of the lift coefficient for $\alpha = 35°$. After a transient region from $0 \le t^* \le 25$, corresponding to the development and advection of the starting vortex, a periodic modulation of the lift coefficient is observed.

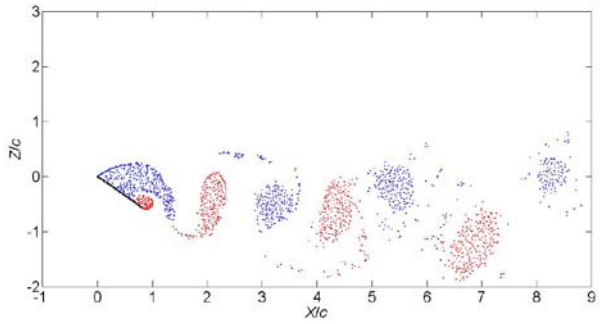

Figure 5. Vortex shedding downstream of a SD7003 airfoil with an angle of attack of 35°.

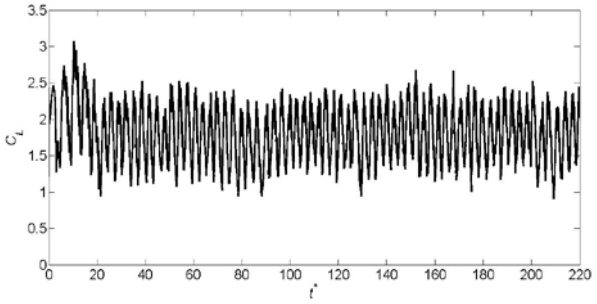

Figure 6. Time development of the lift coefficient of a SD7003 airfoil with an angle of attack of 35°.

A power spectral density function of the lift coefficient is obtained using segment length of 3000 samples and a discrete Fourier transform length of 3000 points. A fundamental peak is observed and its frequency is used to define a Strouhal number associated with the angle of attack as:

$$St_\alpha = f^* \sin\alpha \qquad (32)$$

with f^* the non-dimensional frequency corresponding to the fundamental peak of the power spectral density function.

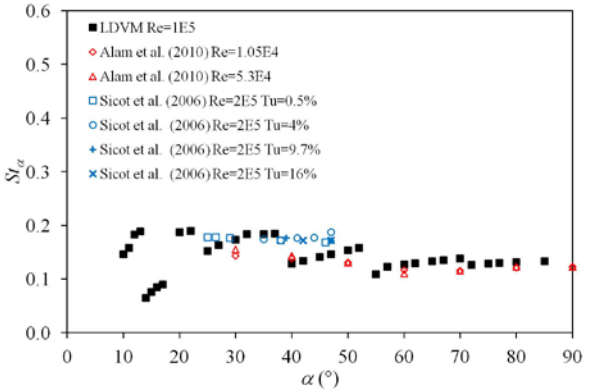

Figure 7. Vortex shedding Strouhal number versus angle of attack for NACA 0012 [12], NACA 65_4-421 [13] and SD7003.

The development of that Strouhal number with angle of attack is plotted in figure 7. Comparison with the

experimental results of [12] conducted with a NACA 0012 airfoil, and [13] conducted with a NACA 65_4-421 airfoil with various upstream turbulence levels are provided. Note that for large values of the angle of attack, the suction side flow is completely detached, and the actual form of the airfoil has little importance, as it is shown by the relative agreement between the points, converging toward a plateau around $St_\alpha = 0.13$.

6. DUAL-AIRFOIL ARRANGEMENT

A dual airfoil arrangement is considered hereafter, with a gap ΔX and a stagger ΔZ between two airfoils of equal chord c (figure 8). The wakes and vortex shedding created by the airfoils and the potential effects between them modifies the flow and the aerodynamic performance of the configuration.

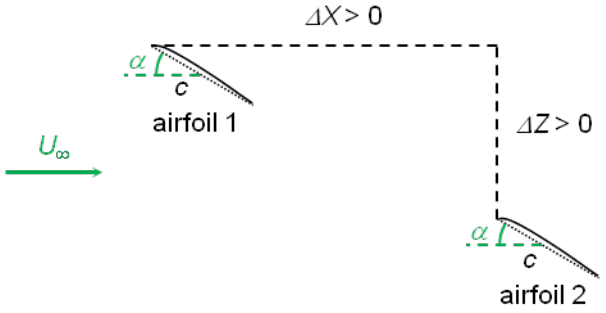

Figure 8. Dual airfoil arrangement with positive gap ΔX and stagger ΔZ.

The arrangement is investigated with the LDVM adapted for two airfoils. For each time step, circulations associated to the TEV and LEV are created, providing four new variables. To solve the problem, the available equations are the LESP criteria for airfoil 1 and 2 and Kelvin's theorem, that is three equations for four unknown parameters:

$$A_{0,1} - \mathrm{LESP}_{crit,1} = 0 \tag{33}$$

$$A_{0,2} - \mathrm{LESP}_{crit,2} = 0 \tag{34}$$

$$\begin{aligned} &\Gamma^*_{B,1} + \Gamma^*_{B,2} + \Gamma^*_{TEV,1,i} + \Gamma^*_{LEV,1,i} + \Gamma^*_{TEV,2,i} + \Gamma^*_{LEV,2,i} \\ &\quad + \sum_{k=1}^{i-1} \Gamma^*_{TEV,1,k} + \sum_{l=1}^{i-1} \Gamma^*_{LEV,1,l} \\ &\quad + \sum_{m=1}^{i-1} \Gamma^*_{TEV,2,m} + \sum_{n=1}^{i-1} \Gamma^*_{LEV,2,n} = 0 \end{aligned} \tag{35}$$

where the indices 1 and 2 are relative to airfoils 1 and 2. An additional condition on Kelvin's theorem is obtained by the initial condition, that is the starting vortex around each airfoil equals zero, replacing (35) by:

$$\begin{aligned} &\Gamma^*_{B,1} + \Gamma^*_{TEV,1,i} + \Gamma^*_{LEV,1,i} + \sum_{k=1}^{i-1} \Gamma^*_{TEV,1,k} \\ &\quad + \sum_{l=1}^{i-1} \Gamma^*_{LEV,1,l} = 0 \end{aligned} \tag{36}$$

$$\begin{aligned} &\Gamma^*_{B,2} + \Gamma^*_{TEV,2,i} + \Gamma^*_{LEV,2,i} + \sum_{m=1}^{i-1} \Gamma^*_{TEV,2,m} \\ &\quad + \sum_{n=1}^{i-1} \Gamma^*_{LEV,2,n} = 0 \end{aligned} \tag{37}$$

Thus, the circulation generation is decoupled in the dual airfoil arrangement by the initial condition imposed by the starting vortex, but the global flow and the advection of the vortices are calculated with all the circulations present at a given time. The linear system of four unknown parameters for four equations is solved with no iterative scheme. The computation of the aerodynamic coefficients for each airfoil is then performed in the same way as for a single airfoil. The velocity field used for the advection is obtained considering the influence of the bound airfoil circulations and all the shed vortices.

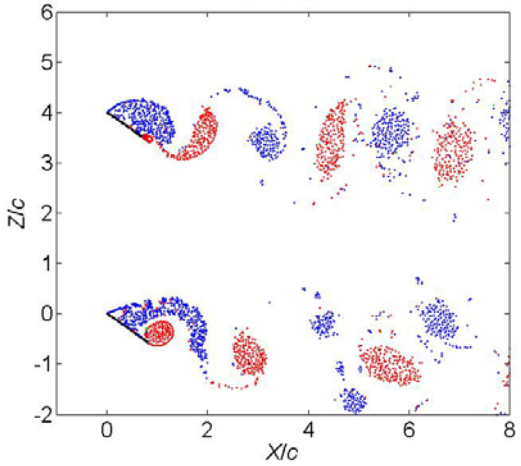

Figure 9. Dual airfoil configuration for gap $\Delta X/c = 0$, stagger $\Delta Z/c = 4$ and angle of attack $\alpha = 35°$.

An example of a LDVM simulation is provided in figure 9 for a Reynolds number $Re = 10^5$, an angle of attack of 35°, a gap $\Delta X/c = 0$ and a stagger $\Delta Z/c = 4$, without vortex clustering downstream of $X/c = 4$. A vortex shedding is developing downstream of each airfoil, but a phase shift is observed in the creation of larger structures, probably due to the potential interaction between the airfoils. Figure 10 is the time development of the flow for a Reynolds number $Re = 10^5$, an angle of attack of 30°, a gap $\Delta X/c = 0.5$ and a stagger $\Delta Z/c = 1.5$. Shortly after starting the flow, at $t^* = 1.5$ (figure 10-a), the suction sides of both airfoils are detached with LEV generation, and the starting vortices are advected downstream. The flows are similar for airfoils 1 and 2. At $t^* = 3$ (figure 10-b), the LEV are developing into large vortices on the suction side, and small discrepancies appear between the airfoils. At $t^* = 4.5$ (figure 10-c), the starting vortices are leaving the field of observation, and a new large TEV is generated. Note the flow discrepancy between the

airfoils, with a change in the leading edge shear layer on airfoil 2. Figures 10-d to f are snapshots for large simulation times t^* between 217.5 and 220.5. Then, the flow is completely established with a periodic vortex shedding. The interaction of airfoil 1 on the leading edge shear layer of airfoil 2 is clearly evidenced.

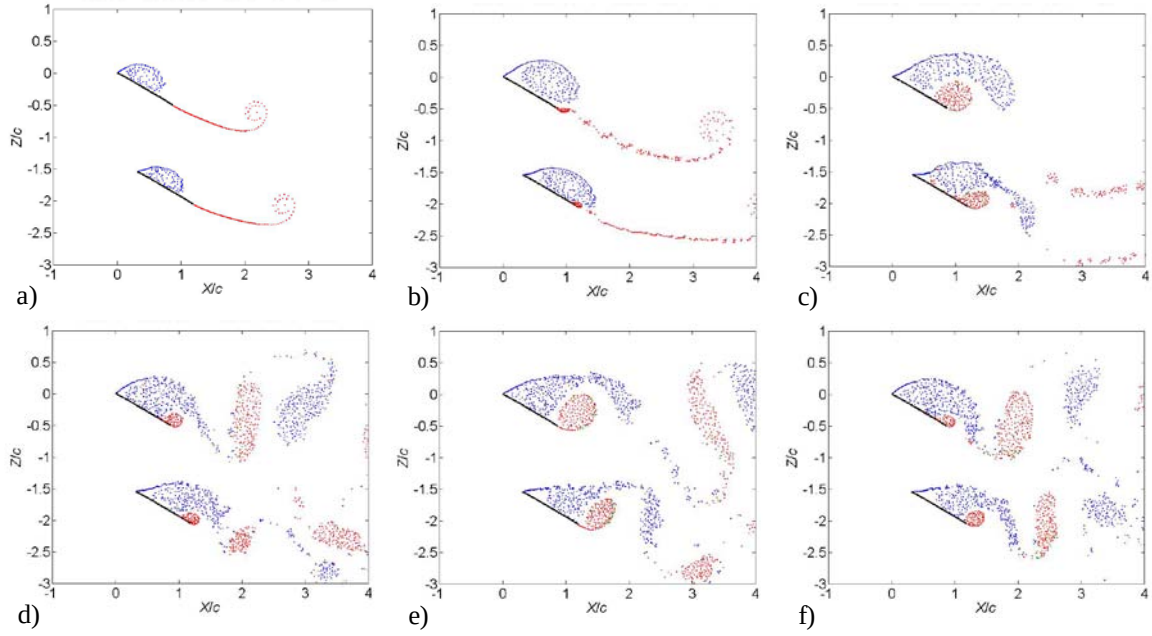

Figure 10. Dual airfoil configuration for gap $\Delta X/c = 0.5$, stagger $\Delta Z/c = 1.5$ and $\alpha = 30°$ for times: a) $t^* = 1.5$, b) $t^* = 3$, c) $t^* = 4.5$, d) $t^* = 217.5$, e) $t^* = 219$, f) $t^* = 220.5$.

7. AERODYNAMIC EFFICIENCY RATIO

In order to quantify the control induced by potential effects or vortex shedding between the airfoils, a systematic study of the lift coefficient is carried out for different gaps and staggers. The lift efficiency ratio is defined, comparing the average lift coefficient for the dual airfoil arrangement $(C_{L,1}+C_{L,2})/2$ with the lift coefficient of the single airfoil configuration $C_{L,s}$, and it is defined from time-averaged values as:

$$R_L = \frac{\overline{C}_{L,1} + \overline{C}_{L,2}}{2\overline{C}_{L,s}} \qquad (38)$$

Figure 11 presents the lift efficiency ratio for a Reynolds number of 10^5, a gap $\Delta X/c = 1.5$ and a stagger $-1 \le \Delta Z/c \le 1$, versus the angle of attack. Comparison is made with the only two-dimensional data available [14] concerning two Wortmann FX63-137 airfoils for a Reynolds number of 8.5×10^4, a gap $\Delta X/c = 1.5$ and a stagger $\Delta Z/c = 0$. A general agreement is found between LDVM and the experiment, although the airfoils considered are different. First of all, a global invariance of the lift efficiency ratio is found with $\Delta Z/c$. The development with the angle of attack is similar, with an increase of the lift efficiency between -5° and 5°, corresponding to attached flow conditions. A very different behavior is found comparing the present results with [15], with an increased lift efficiency for $\alpha \ge 20°$ and $\Delta Z/c \ge 0.5$, but these authors used flat plates with a semi-aspect ratio equal to two, where strong three dimensional effects are expected. Then, the increase observed in that case seems probably due to three dimensional effects.

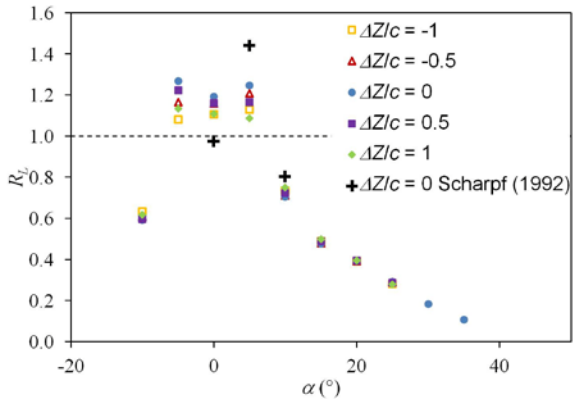

Figure 11. Lift efficiency ratio versus angle of attack for $\Delta X/c = 1.5$ and $-1 \le \Delta Z/c \le 1$.

Preliminary results obtained for a larger gap $\Delta X/c = 3$ seems to prove that the lift efficiency presents a similar behavior with an increase of the efficiency of the dual airfoil arrangement between -5° and 5°.

8. CONCLUSION

The LDVM is implemented successively for the investigation of the unsteady flow around a steady airfoil for large values of the angle of attack. The

method is very similar to the one developed by [3], but without the iteration scheme which is increasing the computing time, since the relevant equations are written as a linear system. The method is validated for three unsteady motions published in [3], and the very same results are found for the vortex shedding morphology and the time development of aerodynamic coefficients. For the steady airfoil case, the results of lift, drag and moment coefficients are compared with the existing data for the SD7003 airfoil. The vortex shedding Strouhal number is found in good agreement with data concerning the flow developing downstream of a detached airfoil. The method is then adapted to the case of two airfoils of equal chord in interaction. To solve the problem, an additional condition is necessary, that is the initial starting vortex condition is written for each airfoil, while the global flow depends on the whole set of shedding vortices. A lift efficiency ratio, comparing lift coefficient resulting from the control between the two airfoils relative to the single airfoil configuration, shows an increase for attached flow conditions between -5° and 5°. These results are in good agreement with the experiments performed with two Wortmann FX63-137 airfoils, in the same Reynolds number range, for a gap equal to zero. A systematic investigation, varying the gap and stagger, is needed to obtain general conclusions on the effective control induced by a dual airfoil configuration. The airfoil shape is also an important parameter. As long as the flow is attached, flow control resulting from the aerodynamic interaction between the airfoils seems to be a good way of improving airfoil performances. For angles of attack larger than 20°, the increase of the lift efficiency ratio observed by [15] seems probably due to three dimensional effects.

9. REFERENCES

[1] Mueller, T.J., DeLaurier, J.D. (2003). Aerodynamics of small vehicles, *Ann. Rev. Fluid Mech.* **35**, 89–111

[2] Sarpkaya, T. (1975) An inviscide model of two-dimensional vortex shedding for transient and asymptotically steady separated flow over an inclined plate, *J. Fluid Mech.* **68** (1), 109-128

[3] Ramesh, K., Gopalarathnam, A., Granlund, K., Ol, M.V., Edwards, J.R. (2014) Discrete-vortex method with novel shedding criterion for unsteady aerofoil flows with intermittent leading-edge vortex shedding, *J. Fluid Mech.* **751**, 500-538

[4] Katz, J., Plotkin, A. (2000) *Low-Speed Aerodynamics*, Cambridge University Press

[5] Vatistas, G.H., Kozel, V., Mih, W.C. (1991) A simpler model for concentrated vortices, *Exp. Fluids*, **11** (1), 73-76

[6] Leonard, A. (1980) Vortex methods for flow simulations, *J. Comput. Phys.* **37** (3), 289-335

[7] Ansari, S.A., Żbikowski, R., Knowles, K. (2006) Nonlinear unsteady aerodynamic model for insect-like flapping wings in the hover. Part 1 methodology and analysis, *Proc. Inst. Mech. Engrs G*, **220** (3), 61-83

[8] Bentley, J.L. (1975) Multidimensional binary search trees used for associative searching, *Communications of the ACM*, **18** (9), 509-517

[9] Ramesh, K., Gopalarathnam, A., Edwards, J.R., Granlund, K., Ol, M.V., (2013) Theoretical analysis of perching and hovering maneuvers, *AIAA Paper*, 23 p.

[10] Selig, M.S., Guglielmo, J.J., Broeren, A.P., Giguère, P. (1995) *Summary of low-speed airfoil data*, SoarTech Publications

[11] Lian, Y., Shyy, W. (2007) Laminar-turbulent transition of a low-Reynolds number rigid of flexible airfoil, *AIAA J.*, **45** (7), 1501-1513

[12] Alam, M.M., Zhou, Y., Yang, H.X., Guo, H., Mi, J. (2010) The ultra-low Reynolds number airfoil wake, *Exp. Fluids*, **48**, 81-103

[13] Sicot, C., Aubrun, S., Loyer, S., Devinant, P. (2006) Unsteady characteristics of the static stall of an airfoil subjected to freestream turbulence level up to 16%, *Exp. Fluids*, **41** (4), 641-648

[14] Scharpf, D.F., Mueller, T.J. (1992) Experimental study of a low Reynolds number tandem airfoil configuration, *J. Aircraft* **29** (2), 231-236

[15] Jones, R., Cleaver, D.J., Gursul, I. (2015) Aerodynamics of biplane and tandem wings at low Reynolds numbers, *Exp. Fluids*, 56:124, 25 p.